Geomechanics and Engineering, *Vol. 19, No. 1 (2019) 49-60*
DOI: https://doi.org/10.12989/gae.2019.19.1.049

Characteristics of EMR emitted by coal and rock with prefabricated cracks under uniaxial compression

Dazhao Song[1], Qiuju You[2], Enyuan Wang*[3], Xiaoyan Song[4], Zhonghui Li[3], Liming Qiu[1] and Sida Wang[1]

[1]School of Civil and Resource Engineering, University of Science and Technology Beijing, Beijing 100083, China
[2]Beijing Research Center of Urban Systems Engineering, Beijing 100035, China
[3]School of Safety Engineering, China University of Mining and Technology, Xuzhou 221116, China
[4]College of Applied Science and Technology, China University of Mining and Technology, Xuzhou 221116, China

(Received March 30, 2018, Revised May 30, 2019, Accepted September 3, 2019)

Abstract. Crack instability propagation during coal and rock mass failure is the main reason for electromagnetic radiation (EMR) generation. However, original cracks on coal and rock mass are hard to study, making it complex to reveal EMR laws and mechanisms. In this paper, we prefabricated cracks of different inclinations in coal and rock samples as the analogues of the native cracks, carried out uniaxial compression experiments using these coal and rock samples, explored, the effects of the prefabricated cracks on EMR laws, and verified these laws by measuring the surface potential signals. The results show that prefabricated cracks are the main factor leading to the failure of coal and rock samples. When the inclination between the prefabricated crack and axial stress is smaller, the wing cracks occur first from the two tips of the prefabricated crack and expand to shear cracks or coplanar secondary cracks whose advance directions are coplanar or nearly coplanar with the prefabricated crack's direction. The sample failure is mainly due to the composited tensile and shear destructions of the wing cracks. When the inclination becomes bigger, the wing cracks appear at the early stage, extend to the direction of the maximum principal stress, and eventually run through both ends of the sample, resulting in the sample's tensile failure. The effect of prefabricated cracks of different inclinations on electromagnetic (EM) signals is different. For samples with prefabricated cracks of smaller inclination, EMR is mainly generated due to the variable motion of free charges generated due to crushing, friction, and slippage between the crack walls. For samples with larger inclination, EMR is generated due to friction and slippage in between the crack walls as well as the charge separation caused by tensile extension at the cracks' tips before sample failure. These conclusions are further verified by the surface potential distribution during the loading process.

Keywords: coal and rock; prefabricated crack; failure mode; electromagnetic radiation; surface potential

1. Introduction

It is well known that coal rock materials due to deformation and rapture emits electromagnetic radiation (EMR). Several investigations showed the relationship between EMR emitted by coal and rock and applied stress on it (Hadjicontis V 1994, Yamada and Oike 1996, Yavorovich *et al.* 2016, Liu *et al.* 2018). Results from theoretical simulations (Chao *et al.* 2012, O'Keefe and Thiel 1995, Rabinovitch *et al.* 2017), experiments (Fukui *et al.* 2005, Mori *et al.* 2004, Song *et al.* 2016), as well as field measurements (Song *et al.* 2017, 2018, Greiling and Obermeyer 2010, Krumbholz *et al.* 2012) suggested that the small-scale fracturing process is the source of EMR.

Nitsan (1977) proposed the piezoelectric effect mechanism. Cress *et al.* (1987) considered that electrostatic charge is distributed on the surface of fragments during fracturing and the rotation, vibration and linear motion of these charged fragments are the main reasons for producing low-frequency EMR, while gas breakdown due to strong electric field produced by charge separation on the fracture surface is the main cause for generation of high-frequency electromagnetic (EM) signals. Ogawa *et al.* (1985) held that the newly broken rock with opposite charges on the two sides is similar to one dipole that emits outward EM signals through charging and discharging. Guo *et al.* (1989) put forth a model showing that EMR is produced by electrons in a perturbed atom. He and Liu (1995) considered that EMR is produced due to combined action of the transient changes in induced electric dipoles, the variable motion of separated charges along fractured edges with cracks propagating and the relaxation of separated charges on the surface of cracks during coal rock deformation and failure. Frid *et al.* (2006) and Rabinovitch *et al.* (2007) presented a feasible EMR model indicating that EMR is produced due to dipole oscillation caused by the surface vibration wave excited by ions' overall motion on both sides during cracks propagation and the amplitude of EMR pulse decreases rapidly due to interaction of a large number of vibration quanta when cracks no longer propagate.

In laboratory studies, Leeman *et al.* (2014) explored the relationship between electrical and mechanical signals for frictional stick-slip events in sheared soda-lime glass bead layers. Gade *et al.* (2014) held the view that EM signals are generated from three different source mechanisms, namely

*Corresponding author, Professor
E-mail: weytop@cumt.edu.cn

Copyright © 2019 Techno-Press, Ltd.

ISSN: 2005-307X (Print), 2092-6219 (Online)

the separation and relaxation of charges during crack growth and the vibration of the charged crack surfaces. Lacidogna *et al.* (2011) investigated the mechanical behaviour of concrete and rocks samples loaded up to their failure by the analysis of acoustic emission (AE) and EMR. AE signals has been always observed during the damage process, whereas the magnetic signals were generally observed only in correspondence to sharp stress drops or the final collapse. Sharma *et al.* (2016) considered that higher frequency of the electric field leads to higher acceleration of the dipoles of the piezoelectric materials, therefore resulting in higher amplitude of EMR. Carpinteri *et al.* (2012) observed energy emission in the form of EMR during the failure process of quasi-brittle materials such as rocks. Kumar *et al.* (2017) and Kumar *et al.* (2018) studied EMR from soft and hard lead zironate titanate (PZT) under the drop weight impact, and suggested that EMR parameters could be used for monitoring excessive deformation from the structures. They also detected EMR from soft PZT under impact at low temperature.

The above theories were derived mostly from laboratory experiments on raw materials or through complicated theoretical derivations and analyses of their mathematical models. Even though they elaborated EMR generating mechanisms from different angles, it is difficult to analyze and verify these mechanisms.

In this paper, we presented two EMR generation mechanisms during coal and rock failure. One is the heterogeneous deformation of Coulomb field caused by charges especially accumulated charges on sample surfaces; the other is the variable motion of charged particles. Both mechanisms result in EMR in the form of a pulse wave (Wang 1997, Wang *et al.* 2009). Because EMR is generated by coal and rock failure or through the cracks development inside the coal and rock mass, we attempt to study the effects of crack propagation on EMR through the prefabricated crack in the coal and rock mass. To this end, we excluded the secondary factors to simplify our analysis and, more importantly, to effectively verify our idea.

Based on the above, we created some samples with prefabricated cracks at different inclinations, and performed uniaxial compression experiments to study the characteristics of EMR emitted from these artificially cracked samples, to explore the effects of prefabricated cracks on EMR generation, and to analyze and verify it using the surface potential signals. This research may provide a brief and effective method for analyzing the law and mechanism of EMR from coal and rock materials.

2. Experimental system and sample fabrication

2.1 Experimental system

Fig. 1 shows the schematic of the acoustoelectric effect experimental system used in the failure process of coal and rocks with prefabricated cracks.

The loading system is a YAW4306 computer-controlled electrohydraulic test machine, and has a maximum load capacity of 3.0×10^3 kN, force resolution of 1/300,000 with relative error rate of 1%, and loading rate of 600-60,000 N/s with accuracy of ±1%. It can be used to automatically record and draw the load displacement curve during loading, and to work out the basic parameters of experimental samples. The acoustoelectric data acquisition system, PCI-2 one, manufactured by Physical Acoustic Corporation is equipped with a board of 18-bit A/D conversion scheme, eight digital I/O, two complete high-speed channels for real time data acquisition, real-time feature extraction, waveform processing and transfer, and frequency response of 3 kHz to 3 MHz at -3 dB points. The LB-IV multi-channel data acquisition system was used to measure the surface potential during coal rock deformation and fracture when being connected with electrode pads. The electromagnetic shielding system is a GP6 electromagnetic shielding room with effectiveness of 14 kHz ≥80 dB, 100 kHz ≥100 dB, 300 kHz ≥110 dB and 50 MHz to 1 GHz ≥110 dB. In addition, to avoid the electromagnetic interference from electricity power, radio wave, and electric equipment, a double copper grid with size less than 0.2 mm was used to cover the coal samples. The coaxial shielded cable was used to connect the sensor and the data recorder.

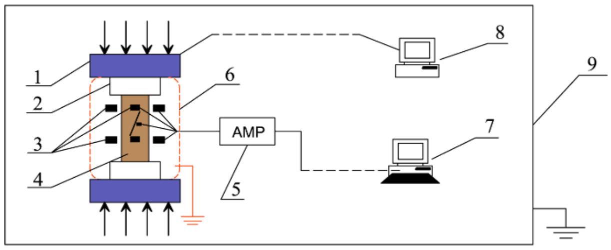

Fig. 1 Schematic of the experimental system 1- Compression testing machine, 2- Insulation pads, 3- Ferrite rod antenna, 4- Coal rock sample, 5- Preamplifiers, 6- Electromagnetic shielding mesh , 7- Data acquisition and processing system, 8- Load control system, 9- Electromagnetic shielding room

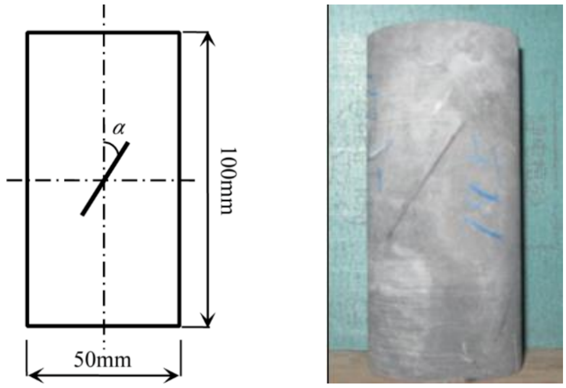

(a) Schematic (b) Photo

Fig. 2 Fabricating of crack

2.2 Sample fabrication

The coal and rock samples were siltstone extracted from No.9 coal seam of Sanhejian Mine of Xuzhou Mining Group, in which mining depth is about 840 m.

The samples were first directly processed into standard cylinder with diameter of 50 mm and length of 100 mm,

Table 1 Experimental parameters of prefabricated crack samples

Type	Mine	Size (mm)	Loading type	Control mode	Loading rate (mm/min)
Coal	Sanhejian	φ50×100	Uniaxial compression	Displacement	0.3
Rock	Sanhejian	φ50×100	Uniaxial compression	Displacement	0.2

(a) Non prefabricated crack (b) Prefabricated crack of 30° inclination (c) Prefabricated crack of 45° inclination (d) Prefabricated crack of 60° inclination

Fig. 3 Photos of samples failed under uniaxial compression

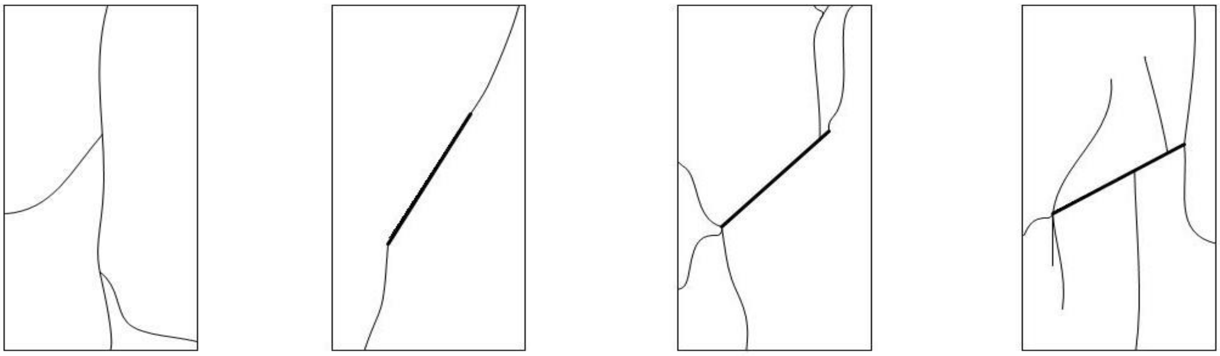

(a) Non prefabricated crack (b) Prefabricated crack of 30° inclination (c) Prefabricated crack of 45° inclination (d) Prefabricated crack of 60° inclination

Fig. 4 Schematics of samples failed under uniaxial compression.

with surface flatness errors at both ends less than 0.02 mm, according to the regulation of the International Society for Rock Mechanics (ISRM); and then selected rigorously by eliminating those samples with obvious damages and visible cracks on their surfaces and those whose size and flatness didn't meet the requirements.

The macroscopic cracks were prefabricated using the mechanically cutting method. The cutting tool was a high-speed electric cutting machine whose rotor blade was a diamond saw of 60 mm diameter and 0.3 mm thickness. The fabricated cracks were about 0.5 mm wide, 25 mm long, and 8 mm deep (the middle position of the crack), shown as Fig. 2(a). All the cracks were single crack on the sample with inclination of 30°, 45° and 60°, respectively. A schematic of the prefabricated crack sample is shown in Fig. 2(a), and its physical picture is shown in Fig. 2(b).

3. Experimental results and analysis

Ten groups of coal and rock samples were tested respectively. Table 1 shows the dtailed experimental parameters of representative coal and rock samples.

3.1 Failure mode of samples

Figs. 3 and 4 show the photos and their correspondent schematics of coal and rock samples suffering deformation and failure under uniaxial compression. It can be seen that the samples with prefabricated cracks of different inclinations present different failure modes, which is in consistence with previously results of other studies (Do *et al.* 2014, Price 2016).

From Figs. 3 and 4(a), the sample without prefabricated crack is completely split generally nearly along the cylindrical axis. The rupture process obviously shows that the sample is of brittleness. At failure, the sample is jittered, and the debris is splashed with audible sound of cracking.

While the sample with prefabricated crack of 30° inclination cracks at its tips. The wing cracks extends along the prefabricated crack, and then turns along the direction parallel to the direction of the maximum principal stress,

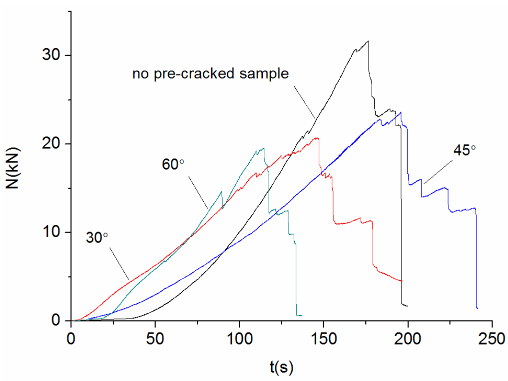

(a) Coal samples

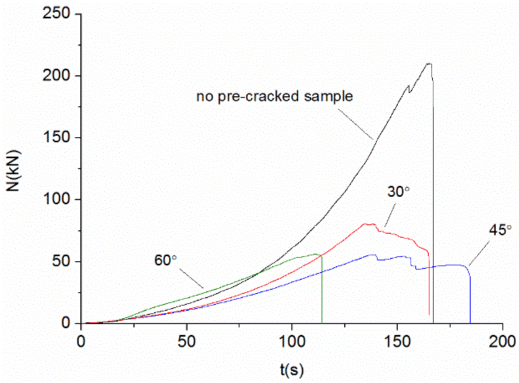

(b) Rock samples

Fig. 5 Relationship of load to time of coal and rock samples failed under uniaxial compression

and lastly extends to both ends, cutting through the whole sample. During wing crack extension, shear cracks first occur at both ends of the prefabricated crack or coplanar secondary cracks with expansion direction coplanar or nearly coplanar to the crack direction. The surfaces of shear cracks or coplanar cracks are rough and have traces of obvious friction. The sample failure originates mainly in the forms of the composite tensile/shear destructions caused by the wing cracks.

As the prefabricated crack inclination increases, as shown in Figs.4(c)-(d), the wing cracks appear at the early stage, extend to the direction of the maximum principal stress, and eventually run through both ends of the sample, resulting in the sample's failure. The wing cracks have smooth, clean surfaces and no fragmentation-like substances, thus they are tension cracks. At the same time, reverse wing cracks or shear cracks also present themselves. The sample eventually fails due to tension.

It is shown that the prefabricated crack is the main factor leading to failure of the sample. After loading, due to the stress concentration effect in the prefabricated crack region, the sample first breaks at both ends of the crack, then wing cracks present themselves. As loading increases, the wing cracks ceaselessly extended till run through the sample, resulting in its full failure. The extension of wing cracks mainly orients at two directions: one is along the prefabricated crack direction and the other is vertical to the crack direction.

3.2 Relationship of load to time in samples with a prefabricated crack

In order to study the relationship between EM signal and the loading path and to analyze its characteristics in various stages, the load-displacement curves of coal and rock samples (Batch 0117 coal sample and Batch 0106 rock sample) are shown as Figs. 5(a) and 5(b), respectively.

As shown in Fig.5, as the sample's skeleton structure has been destroyed by the prefabricated crack to some extent, its loading capacity decreases greatly. The effects of the crack on the coal and rock sample strengths are different. For the coal sample, its uniaxial compressive strength decreases from 30 kN to 20 kN, dropping by an average of 33.3%, while for the rock sample, its decreases from 200 kN to 60 kN, dropping by an average of 70%. In addition, compared to the sample without prefabricated crack, the loading duration of the sample with a 30° crack is similar, while that of 60° reduces by about 30 %, and that of 45° is much longer. This is due to the minimum inclination between the 30° prefabricated crack and the principal stress direction, resulting in the smallest effect on the strength and loading duration, while with the inclination of cracks increasing, the projection of the crack on the cylindrical section is larger, that is, failure surface is appreciable, leading to the change of the sample's strength.

3.3 EMR characteristics

3.3.1 Coal sample

In the experiments, we chose the EMR sensor with receiving frequency of 300 kHz. Fig.6 shows the results of Batch 0117 coal sample, which loading-time curve corresponds to Fig. 5(a).

From Fig. 6(a) it is seen that the EM signal emitted from non-prefabricated crack has very relationship to the loading. At 140s-150s, the sample enters the accelerated inelastic failure stage, and the EM signals increase rapidly.

In Fig. 6(b), the presence of prefabricated crack at inclination of 30°, which is equivalent to the increase in the transverse activity space among the skeleton's load-bearing structure inside the sample, could increase the capacity of the sample's elastic deformation and simultaneously lower the friction and press among the adjacent structures. Therefore, the corresponding EM signal during the early stage is relatively calm. According to Section 3.1, the shear cracks are dominant in the development of wing cracks caused by the prefabricated crack. Thus, pressing, friction, and slipping among the microscopic particles on the crack surface are also overwhelming during shear cracks propagation. As a result, the EM signal in this stage should be rich and continuous.

In Fig. 6(c), in the initial loading, the EMR signal is also relatively smooth. After 200 seconds, the loading increases rapidly and the signal raises up suddenly due to the close contact and relative movement between two walls of the crack. At 295 seconds, the loading reaches its maximum, so does the signal. After that, in the fluctuating stage of softening, the signal shows fluctuating peaks, suggesting that in this stage, with the loading waving, the high intensity fluctuation signal is observed due to friction and slipping between the wall surfaces of sample cracks.

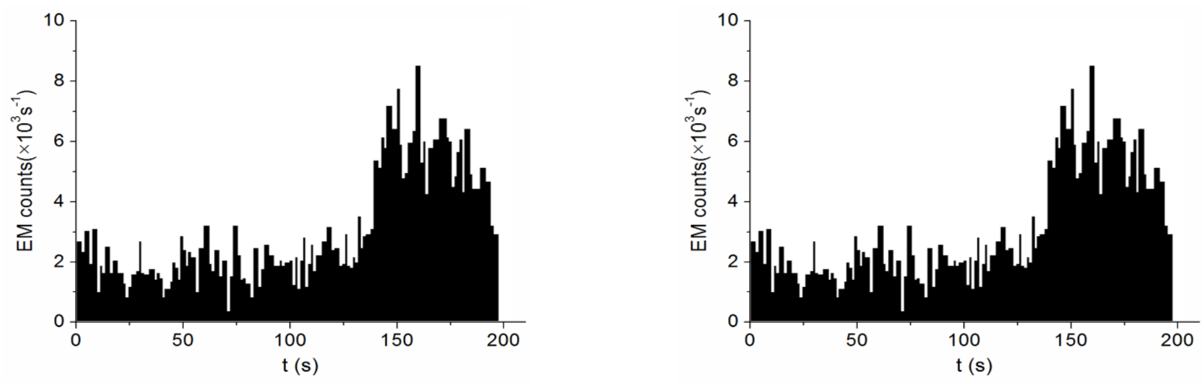

(a) The sample without prefabricated crack

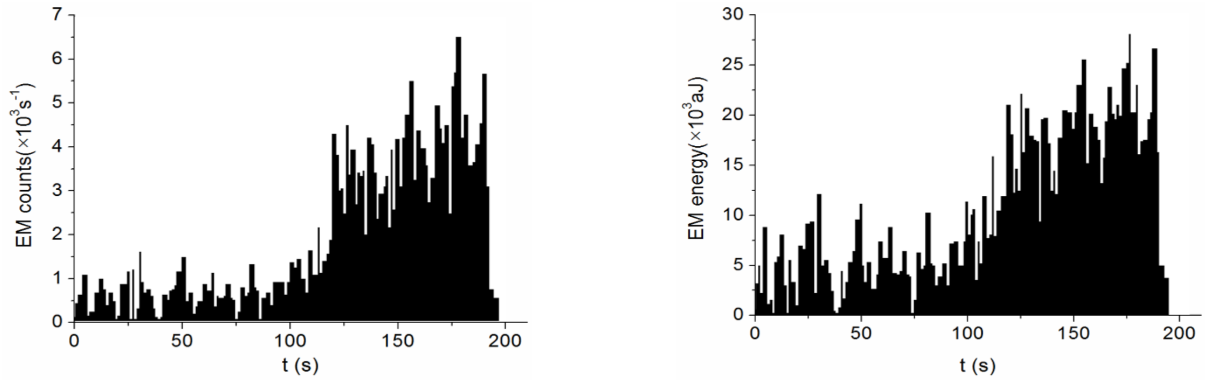

(b) The samples with prefabricated cracks of 30° inclination

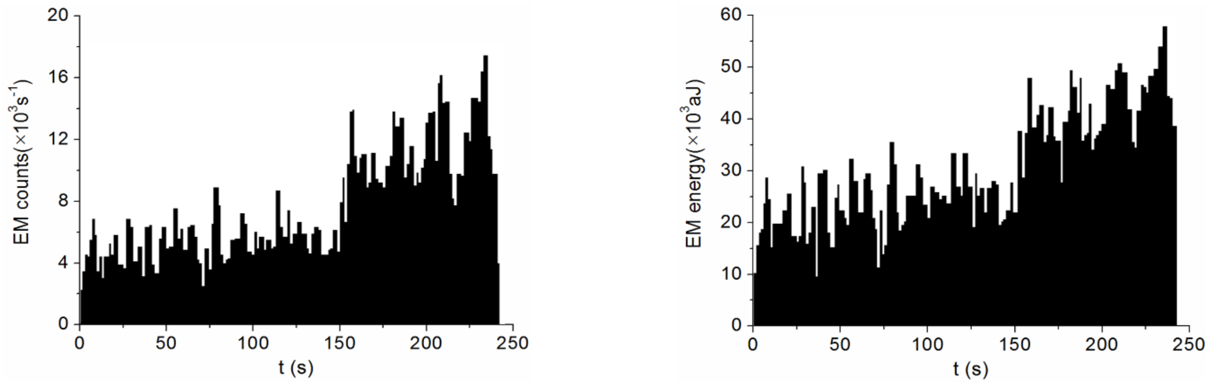

(c) The samples with prefabricated cracks of 45° inclination

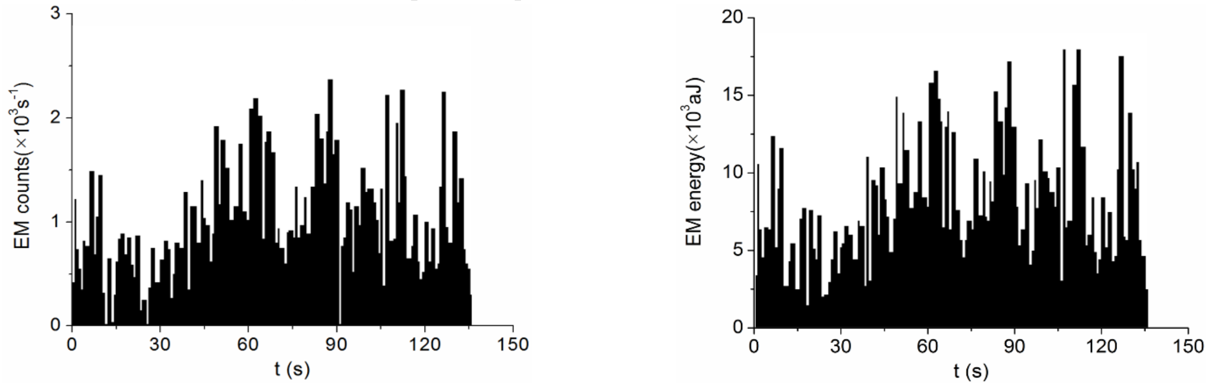

(d) The samples with prefabricated cracks of 60° inclination

Fig. 6 EM counts and energy generated by coal sample during uniaxial compression

From Fig. 6(d) it is clear that the EM signal is characteristic of multimodal. We believe that under uniaxial compression, the two wall surfaces of the prefabricated crack with 60° inclination bear greater compressive stress and there is no any filling in the prefabricated crack. Thus, two wall surfaces have been completely compacted in a

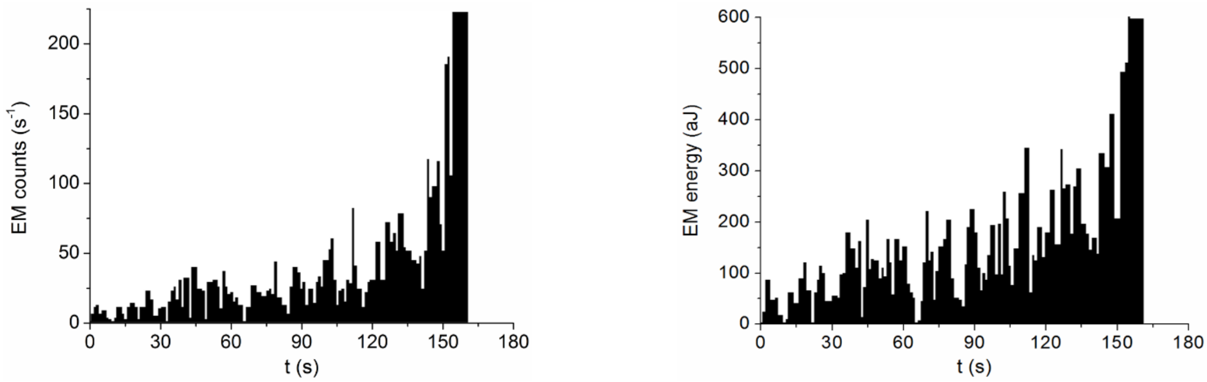

(a) The sample without prefabricated crack

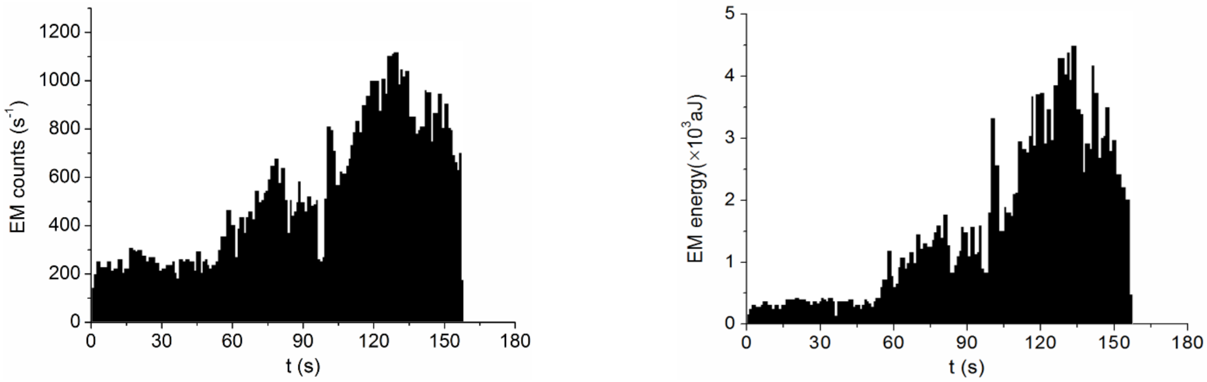

(b) The samples with prefabricated cracks of 30° inclination

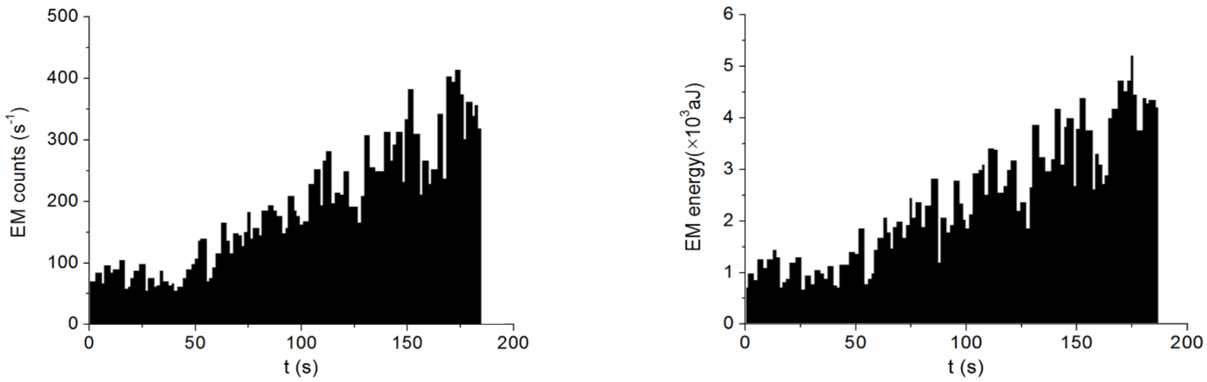

(c) The samples with prefabricated cracks of 45° inclination

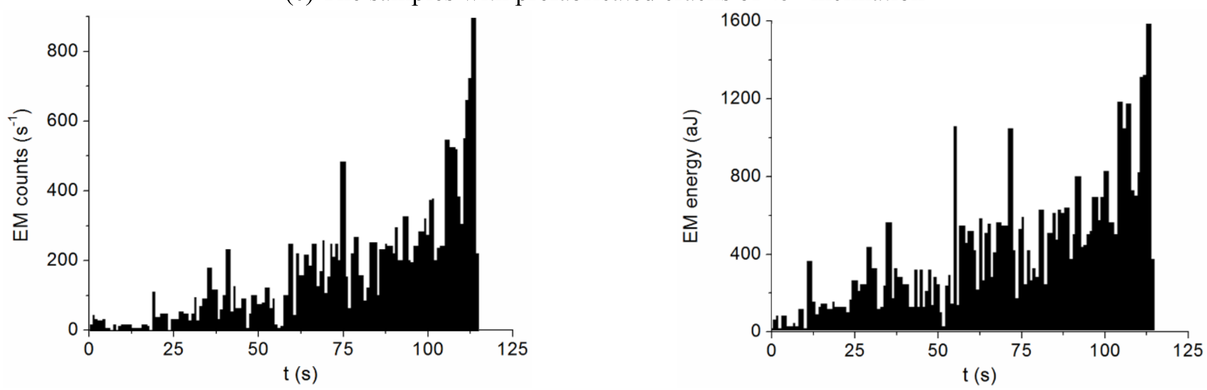

(d) The samples with prefabricated cracks of 60° inclination

Fig. 7 EM counts and energy generated by rock sample during uniaxial compression

smaller loading, and the strong slipping and friction between two wall surfaces result in the emitting of a large quantity of EMR. After full compaction, the axial bearing capacity of the sample increases to some extent, and the radial extension of wing cracks is blocked. In the crack wall appear the axial secondary cracks whose generation and

Table 2 Characteristics of EMR stages of failure process of coal samples

Inclinations	Crack compaction stage	Crack stable propagation stage	Crack instable failure stage	Macrocrack development stage
0°	fluctuation	fluctuation growth	rapid growth	peak concentration
30°	fluctuation	fluctuation growth	rapid growth	peak concentration
45°	fluctuation	fluctuation growth	rapid growth	peak concentration
60°	fluctuation	fluctuation	fluctuation peak	fluctuation

Table 3 Characteristics of EMR stages of failure process of rock samples

Inclinations	Crack compaction stage	Crack stability propagation stage	Crack instability failure stage	Macrocrack development stage
0°	calmness	fluctuation growth	peak concentration	-
30°	fluctuation growth	rapid growth	peak concentration	-
45°	fluctuation growth	rapid growth	peak concentration	-
60°	fluctuation growth	rapid growth	peak concentration	-

propagation need energy accumulation, so the EM signal is also stronger. In other words, the samples with prefabricated cracks at larger inclination can generate EM signal from beginning to the end during the loading. In the early stage, it is generated mainly due to relative movement between the closely compacted wall surfaces, while in the late stage it is mainly produced during crack propagation.

It is seen that the prefabricated crack is the main factor causing the coal sample damages. Accordingly, the sliding and friction between the wall surfaces, as well as the crack propagation and instability are the main reasons of EMR generation in the whole process of the sample's failure.

3.3.2 Rock sample

In the experiments, we chose the EMR sensor with receiving frequency of 25 kHz. Fig. 7 shows the measurement results of Batch 0106 rock sample with corresponding loading-time curve shown in Fig. 5(b).

By comparing Figs. 6 and 7, it can be seen that the EMR emitting law of rock subject to uniaxial compression are similar to that of coal in the same condition. But there are also some differences. EMR from coal samples is richer and more complex and often coupled with multimodal phenomenon, while that from rock samples is characteristic of relative concentration, and, generally speaking, increases rapidly with loading increasing and disappearing fast with loading softening.

3.3.3 Comparison of EMR of coal and rock failure

From the view of crack propagation, the whole failure process of coal and rock samples under uniaxial compression can be divided into four stages: crack compaction, crack stable propagation, crack instable propagation, and macrocrack development. Correspondingly, the EM signals in these four stages are different and summarized as characteristics of calmness, fluctuation growth, rapid growth, and peak concentration, shown in Table 2 and 3. Based on them, we further analyzed the influence of prefabricated cracks with different inclinations on the fracture process, and subsequently on EM signals.

Comparing the characteristics of EMR at various stages of coal and rock failure process in Tables 2-3 and combining Figs. 7-8, we found that:

(1) From the view of crack propagation, the whole failure process of coal and rock samples can be divided into 4 stages. The EM signals in these stages have different phase characteristics.

In the crack compaction stage, the EMR is mainly caused by crack closure, and the signals are scarce or absent. During the crack stable propagation stage, the EMR tends to be active, and the signal increases continuously. After entering the crack instable failure stage, the microcracks of the sample aggregate and coalesce, gradually forming macrocracks. The EMR is extremely active, and reaches the maximum near the peak stress. Subsequently, the EMR disappears gradually. Therefore, the EM signals can effectively reflect the morphological changes within the coal and rock, inversing the whole microscopic process from crack formation and evolution to coalescence and formation of macrocracks as well as failure.

(2) Compared to the common samples, the EMR staging characteristics of the samples with prefabricated crack have the tendency of forward movement, which are more obvious in the coal samples of 60° inclination and all rock samples.

As shown in Table 2, for coal samples, the influence of prefabricated cracks on the EM signal is limited. At each stage, the EMR characteristics of the samples with prefabricated cracks of 30 or 45 inclinations are very similar to those of samples without prefabricated crack. This may be because the coal sample itself has more internal defects. Compared with these defects, prefabricated cracks cannot show absolute advantages in the process of absorbing external energy. In other words, the contribution of the prefabricated cracks to the instable failure is submerged in a large number of primary defects in the coal samples. For the sample of larger inclination (60°), the crack damages larger cross-sections. According to the statistical damage theory, only the intact skeleton in the vicinity of the cracks is subjected to the loads. In this way, smaller stresses can cause tensile stresses at the prefabricated crack tip to produce EMR. At this point, such a small pressure has not even reached the minimum strength to extend the primary fracture in the samples. The prefabricated cracks are absolutely advantageous in absorbing external energy and expanding itself. As the load continues to increase, the primary fracture begins to expand. According to Fig. 5, the "fluctuation" in samples with 60° prefabricated crack in the compaction stage is caused by the change of the precrack tips and the "fluctuation" of the crack in the propagation stage, is the result of the combination of the prefabricated crack and the primary defects. After that, the EMR jumps to the "rapid growth" phase and rapidly enters the fluctuating peak state.

For rock samples, due to their good homogeneity and fewer internal defects, the prefabricated cracks of various inclinations occupy the dominant position in the instable failure of the sample from beginning to end. At the same time, as the crack effectively reduces the strength of the sample, the EMR in the whole process shows characteristics of a “clam” phase in advance of the four stages of the crack propagation, shown as the calmness in the sample without crack in Table 3.

It can be seen that the stage characteristics of EM signal are closely related to the crack propagation and failure process.

4. Discussion

4.1 Role of prefabricated crack in EMR generation

Through the above analysis, the characteristics of EMR are closely related to the crack propagation and fracture process. So we try to discuss the role of prefabricated crack in EMR generation.

In the presence of prefabricated crack, the sample’s deformation and failure are not wholly random. They mainly initiate from both ends of the prefabricated crack, and from the ends form wing cracks which rapidly develop along two directions.

When the inclination of prefabricated crack is small, the shear cracks or coplanar secondary cracks first appear at its two tips and then propagate along coplanar or nearly coplanar direction of the prefabricated crack, tending to shear failure. The surfaces of shear cracks or coplanar cracks are rough and have obvious friction traces. The coal and rock materials are composed of mineral particles and cements. These materials are combined by weaker Van der Waals force, thus the coal and rock masses subject to loading produce free charges due to sliding, dislocation, and friction among these composites. When the crack rapidly split, the charges on the both sides of the double electric layer couldn’t completely disappear, thus forming separated charges, and their motion emits outward EM wave (Alekseev *et al.* 1993, Ivanov *et al.* 1988, Liu *et al.* 1997, Nardi and Caputo 2009, Zhu *et al.* 1998). It is evident that the contribution of friction to EMR depends upon the shear inclination of the crack. The smaller the inclination is, the higher the proportion produced by friction. This kind of electrification phenomenon lasts in the entire process of shear failure.

When the inclination is large, the sample mainly undergoes tensile failure. When the prefabricated crack closes, secondary cracks generally present themselves around it. The cracks’ tensile expansion is mainly limited to the range of atomic scale around the cracks’ tips, in which intergranular cracking and transgranular cracking occur. The intercrygranular cracking mainly occurs in the granular boundary, making the van der Waals force change, i.e., making the intergranular potential change. The transgranular cracking causes break of chemical bonds, producing a larger quantity of charges (Rosen 1964, Zweben and Rosen, 1970). Furthermore, the cracks and defects in coal rock materials under external force may cause local stress concentration, making the kinetic energy of locally bound electrons increase and causing them to escape and become free electrons (Hoxha 2005, Krajcinovic 1989). It is just because different deformations of various parts in the coal rock materials that result in different distributions of charges generated therein and cause EMR to be emitted. The experiment found that EMR signal emitted by the sample with larger prefabricated crack more easily shows outburst and multi-peak phenomena. These phenomena account for instantaneous dissipation and release of energy caused mainly by tensile failure (Cao *et al.* 2015, Qian *et al.* 1986)

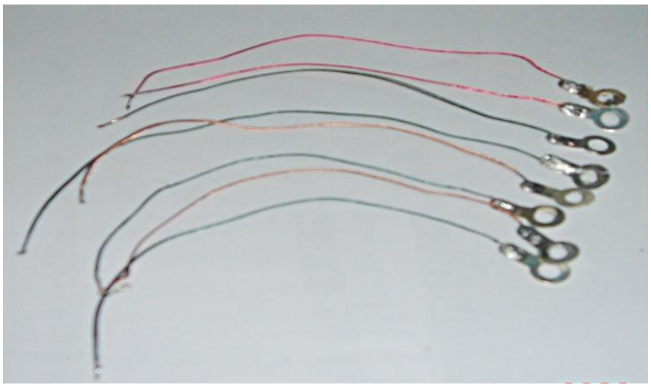

Fig.9 Physical pictures of electrode pads

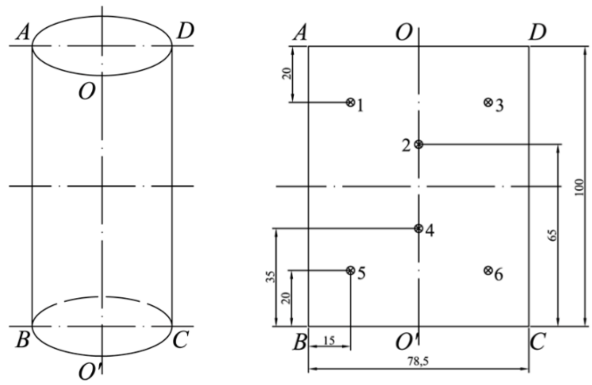

(a) Schematic of sample (b) Front surface of sample

Fig. 10 Schematic of copper plate electrodes distribution

Impacted by the prefabricated crack with different inclinations, the sample in different modes of destruction has different mechanisms of EMR generation. When the inclination is smaller, the variable motion of free charges generated due to crushing, friction, and sliding in between the crack walls is the main reason of EMR generation. While when the inclination is bigger, the charge separation caused by tensile extension at the cracks’ tips in this region is the main contributor to rapid increase EMR in the later loading stage.

4.2 Surface potential experiment of prefabricated crack

From the above, free charges are the main reason of EMR generation during deformation and failure of coal and rock. Impacted by prefabricated cracks, free charges generated by different forms and at different positions under different manner of destruction contribute differently to EMR.

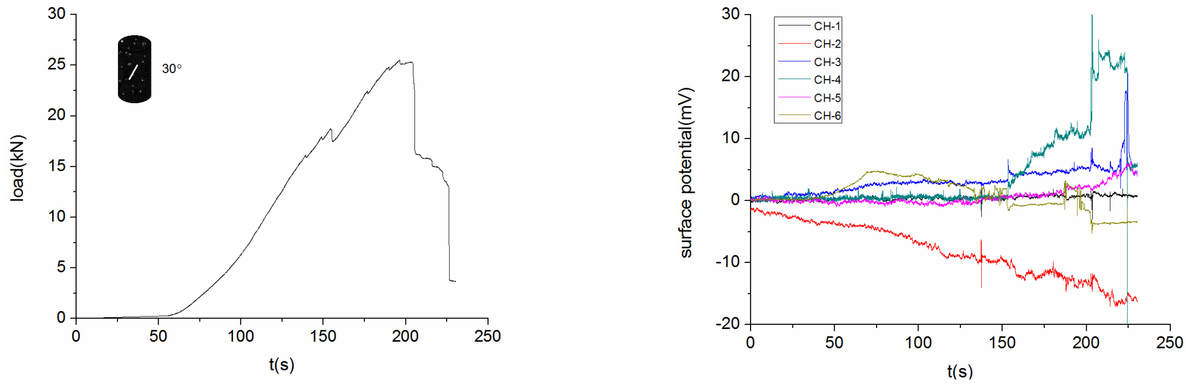

(a) (b)

Fig. 11 Prefabricated crack of 30° inclination

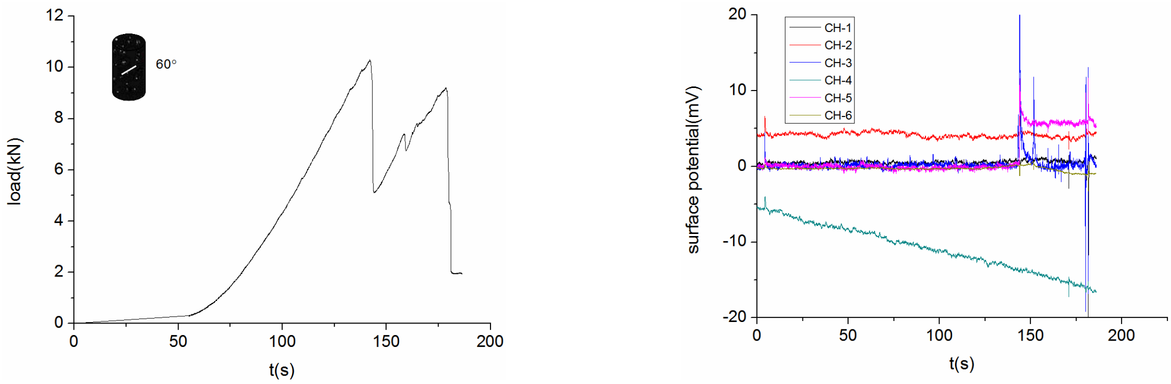

(a) (b)

Fig.12 Prefabricated crack of 60° inclination

In order to verify our idea of the role of prefabricated crack in EMR generation, we placed electrode pads around prefabricated crack to measure the potential signal during loading.

4.2.1 Experiment scheme

In this experiment, we used LB-IV multichannel potential date acquisition system. The system mainly consists of a central controller, a data acquisition, and a front-end bridge amplifier and is equipped with 28 acquisition channels that can be used to connect electrode pads and strain gauges to measure the surface potential or strain during deformation and fracture of coal and rock mass.

The physical picture of the electrode pads is shown in Fig. 9. The distribution and locations of these pads are shown in Fig.10, in which Fig.10 (b) shows the half of the front panel of pads in Fig.10 (a) in front of the sample column. In the experiment, the positions of batches No. 1-6 in Fig.10 (b) were connected with channels 1-6, respectively.

4.2.2 Results and analysis

According to Section 3.3, it is obvious that many factors attribute to EMR generation from samples with prefabricated crack of 30 and 60° inclinations. In this paper, we only discuss the surface potential signals generated by these samples. Fig.11 and Fig.12 show the typical results.

From Fig.11, with loading gradually increasing, the absolute values of surface potential signals measured by 6 channels, in a whole, also increase correspondently, but their increasing ways are different.

The signal from Channel No.1 changes slightly, indicating that there are smaller native defects in the region. During the sample's destruction, the region stays always in the stage of elasticity and no great cracking occurs. Therefore, only a small amount of free charges are generated.

The signals received from Channels No. 3, 5, and 6 change slowly during overall loading; after the main rapture, the signal increment grows significantly, which originates in that the extensions of native defects and cracks caused by the main rapture in the correspondent regions, leading to more charge separation. During loading after the signal peak, the signal again becomes smooth but stays at relatively higher level till the sample undergoes the second rapture and final failure.

What received by Channels No.2 and 4 are the potential signals emitted from the two sides of the prefabricated crack. During overall loading, the signals of these two channels grow gradually, and accelerate faster in the later stage, indicating that the contact and friction of crack walls in the later stage produce more signals. What's more, their increments are much greater than those obtained by the other 4 channels, showing that the free charges generated in these regions corresponding to these two channels are the most and continuous. Because these two channels are located at the both sides of the prefabricated crack, we have sufficient reasons to believe that the great changes in potential signals of these two channels are resulted from a large amount of continuous free charges generated by sliding, dislocation, and friction in between the two closely compacted walls of the prefabricated crack subject to loading.

At the same time, the negative charges and the positive charges measured by Channels No. 2 and 4, respectively, fully prove from another angle that the positive and negative charge separation is caused by friction between the prefabricated crack's walls. As viewed from the potential signal strength, the quantity of free charges measured from the two wall surfaces of the prefabricated crack is much greater than that from other regions, thus the most contribution made to EMR generation comes from the free charges produced in between the two wall surfaces of the prefabricated crack.

Fig. 12 (a) is a common curve shape of samples with 60° prefabricated crack during loading, which usually has two peaks. The former peak is caused by tension rupture at both ends of the prefabricated crack under external loads, and then unloaded rapidly. However, the sample has not been completely destroyed at this time. After the crack closes, it can still withstand a certain load until it continues to be final failure.

Different failure modes lead to the difference generating positions and change trends of surface potential signals between the samples with 60° and 30° prefabricated cracks. From Fig.12 it is clear that the signals from Channels No.1 and 6 are very small and their variations are not obvious, which indicates that there is no great damage and destruction in these two regions during loading. More potential signals are still measured from Channels No.2 and 4 located at the two sides of the prefabricated crack, especially after tension failure occurs at both ends of the crack, which means that for the sample with the prefabricated crack of big inclination, the sliding and friction still occur in between its two wall surfaces after contacting each other, resulting in the generation of a significant number of free charges.

In comparison with Fig.11, the signals from Channels No.3 and 5 are most evident. According to the analysis of Section 3.1-3.2, we know that on the both sides of the sample's prefabricated crack of 60° inclination, the tensile destruction is dominant, after it closure, the secondary cracks occur at its two ends. Channels No.3 and 5 are responsible for measuring the signals generated from the extension regions of the two ends of the prefabricated crack. As viewed from Fig. 12(a), the sample during loading produces two obvious load peaks, and the potential signal is in good agreement with Fig. 12(b). It is seen that instantaneous tensile extension and failure from which the prefabricated crack suffers result in the generation of a large quantity of free charges, thus the tensile extension at the tips of the prefabricated crack possesses important contribution to EMR.

It is worth noting that the surface potential signals from Channels No.3 and 5 before and after the peak have evident fluctuation, but through statistics, during the overall deformation and failure of the sample, the free charges generated in the vicinity of two wall surfaces of the prefabricated crack are much more. A possible explanation is that the sliding and friction in between two wall surfaces of the prefabricated crack only are persistent charge separation processes, while the crack propagation incites the instantaneous release of free charges. In other words, the most contribution to EMR during overall process from sample loading to full failure comes from the free charges generated by the relative motion in between the wall surfaces of the prefabricated crack; the main contributor to the EMR peak to which the sample peak destruction corresponds is the free charges separated by the tensile destruction at the tips of the prefabricated crack.

5. Conclusions

We carried out the uniaxial compression experiments on coal and rock samples with prefabricated cracks of different inclinations, measured EM signals generated from them, studied the effects of the prefabricated crack on EMR, and verified it by measuring the surface potential signals. The main conclusions are as follows:

(1) Prefabricated cracks are the main factors leading to the failure of coal and rock samples.

a. When the inclination between prefabricated crack and axial stress is smaller, the wing cracks occur first from the two tips of the prefabricated crack, and expand to shear cracks or coplanar secondary cracks whose advance directions are coplanar or nearly coplanar with the prefabricated crack's direction. The sample failure is mainly due to the composite tensile and shear destructions caused by the wing cracks.

b. When the inclination becomes bigger, the wing cracks appear at the early stage, extend to the direction of the maximum principal stress, and eventually run through the both ends of the sample, resulting in the sample's tensile failure.

(2) The effect of samples with prefabricated cracks of different inclinations on EM signals is different.

a. For prefabricated crack of smaller inclination, the variable motion of free charges generated due to crushing, friction, and slippage between the crack walls is the main reason of EMR generation.

b. Bigger inclination has 2 aspect of influences: friction and slippage etc. in between the crack walls in the early stage; and the charge separation caused by tensile extension at the cracks' tips before sample failure. The surface potential distribution during the loading process verifies the above conclusions.

(3) Our results advance the research of EMR theory of coal rock from the statistical correlation of stress-EMR to the direct relationship between fracture and EMR, and provide a new mean and idea for quantitative revealling the EMR mechanism of coal and rock failures, thus enriching the theoretical basis for better application of this technology in monitoring and early warning of coal rock dynamic hazards.

Acknowledgments

This work is supported by the National Natural Science

Foundation of China (51774023, 51634001), Beijing Nova Program (xx2018073), and Fundamental Research Funds for the Central Universities (FRF-TP-16-071A1).

References

Alekseev, D.V., Egorov, P.V. and Ivanov, V.V. (1993), "Mechanisms of electrification of cracks and electromagnetic precursors of rock fracture", *J. Min. Sci.*, **28**(6), 515-519. https://doi.org/10.1007/BF00734067.

Bagheripour, M.H., Rahgozar, R., Pashnesaz, H. and Malekinejad, M. (2011), "A complement to Hoek-Brown failure criterion for strength prediction in anisotropic rock", *Geomech. Eng.*, **3**(1), 61-81. http://dx.doi.org/10.12989/gae.2011.3.1.061.

Cao, P., Liu, T., Pu, C. and Lin, H. (2015), "Crack propagation and coalescence of brittle rock-like specimens with pre-existing cracks in compression", *Eng. Geol.*, **187**, 113-121. https://doi.org/10.1016/j.enggeo.2014.12.010.

Carpinteri, A., Lacidogna, G., Borla, O., Manuello, A. and Niccolini, G. (2012), "Electromagnetic and neutron emissions from brittle rocks failure: Experimental evidence and geological implications", *Sadhana*, **37**(1), 59-78. https://doi.org/10.1007/s12046-012-0066-4.

Chao, W., Xu, J., Zhao, X. and Wei, M. (2012), "Fractal characteristics and its application in electromagnetic radiation signals during fracturing of coal or rock", *Int. J. Min. Sci. Technol.*, **22**(2), 255-258. https://doi.org/10.1016/j.ijmst.2012.03.003.

Cress, G.O., Brady, B.T. and Rowell, G.A. (1987), "Sources of electromagnetic radiation from fracture of rock samples in the laboratory", *Geophys. Res. Lett.*, **14**(4), 331-334. https://doi.org/10.1029/GL014i004p00331.

Do, N.A., Dias, D., Oreste, P. and Djeran-Maigre, I. (2014), "2D numerical investigations of twin tunnel interaction", *Geomech. Eng.*, **6**(3), 263-275. http://dx.doi.org/10.12989/gae.2014.6.3.263.

Frid, V., Rabinovitch, A. and Bahat, D. (2006), "Crack velocity measurement by induced electromagnetic radiation", *Phys. Lett. A*, **356**(2), 160-163. https://doi.org/10.1016/j.physleta.2006.03.024.

Fukui, K., Okubo, S. and Terashima, T. (2005), "Electromagnetic radiation from rock during uniaxial compression testing: the effects of rock characteristics and test conditions", *Rock Mech. Rock Eng.*, **38**(5), 411-423. https://doi.org/10.1007/s00603-005-0046-7.

Gade, S.O., Weiss, U., Peter, M.A. and Sause, M.G.R. (2014), "Relation of electromagnetic emission and crack dynamics in epoxy resin materials", *J. Nondestruct. Eval.*, **33**(4), 711-723. https://doi.org/10.1007/s10921-014-0265-5.

Greiling, R.O. and Obermeyer, H. (2010), "Natural electromagnetic radiation (EMR) and its application in structural geology and neotectonics", *J. Geol. Soc. India*, **75**(1), 278-288. https://doi.org/10.1007/s12594-010-0015-y.

Guo, Z.Q. (1989), "The model of compressed atoms and electron emission of rock fracture", *Chin. J. Geophys.*, **32**, 73-117.

Hadjicontis V.M.C. (1994), "Transient electric signals prior to rock failure under uniaxial compression", *Geophys. Res. Lett.*, **21**(16), 1687-1690. https://doi.org/10.1029/94GL00694.

Han, J., Huang, S., Zhao, W., Wang, S., and Deng, Y. (2018), "Study on electromagnetic radiation in crack propagation produced by fracture of rocks", *Measurement*, **131**, 125-131. https://doi.org/10.1016/j.measurement.2018.06.067.

He, X.Q. and Liu, M. (1995), *Electro-magnetic Dynamics of Coal or Rock Containing Gas*, University of Mining and Technology Press, Xuzhou, China.

Hoxha, D., Lespinasse, M,. Sausse, J. and Homand F. (2005), "A microstructural study of natural and expermentally induced cracks in a granodiorite", *Tectonophysics*, **395**, 99-112. https://doi.org/10.1016/j.tecto.2004.09.004.

Ivanov, V.V., Egorov, P.V., Kolpakova, L.A. and Pimonov, A.G. (1988), "Crack dynamics and electromagnetic emission by loaded rock masses", *Soviet Min.*, **24**(5), 406-412. https://doi.org/10.1007/BF02498591.

Krajcinovic, D. (1989), "Damage mechanics", *Mech. Mater.*, **8**(2-3), 117-197. https://doi.org/10.1016/0167-6636(89)90011-2.

Krumbholz, M., Bock, M., Burchardt, S., Kelka, U. and Vollbrecht, A. (2012), "A critical discussion of the electromagnetic radiation (EMR) method to determine stress orientations within the crust", *Solid Earth*, **3**(2), 401-414. https://doi.org/10.5194/se-3-401-2012.

Kumar, A., Chauhan, V. S., Sharma, S. K., and Kumar, R. (2017), "Deformation induced electromagnetic response of soft and hard PZT under impact loading", *Ferroelectrics*, **510**(1), 170-183. https://doi.org/10.1080/00150193.2017.1328726.

Kumar, S.S., Kumar, S.A., Chauhan, V.S. and Michael, S. (2018), "Effect of low temperature on electromagnetic radiation from soft pzt sp-5a under impact loading", *J. Elect. Mater.*, **47**(10), 5930-5938. https://doi.org/10.1007/s11664-018-6464-6.

Lacidogna, G., Carpinteri, A., Manuello, A., Durin, G., Schiavi, A. and Niccolini, G. and Agosto, A. (2011), "Acoustic and electromagnetic emissions as precursor phenomena in failure processes", *Strain*, **47**(s2), 144-152. https://doi.org/10.1111/j.1475-1305.2010.00750.x.

Leeman, J.R., Scuderi, M.M., Marone, C., Saffer, D.M. and Shinbrot, T. (2014), "On the origin and evolution of electrical signals during frictional stick slip in sheared granular material", *J. Geophys. Res. Solid Earth*, **119**(5), 4253-4268. https://doi.org/10.1002/2013JB010793.

Liu, X. and Wang, E. (2018), "Study on characteristics of EMR signals induced from fracture of rock samples and their application in rockburst prediction in copper mine", *J. Geophys. Eng.*, **15**(3), 909-920. https://doi.org/10.1088/1742-2140/aaa3ce.

Liu, Y., Liu, Y., Wang, Y., Jin, A., Fu, J. and Cao, J. (1997), "The influencing factors and mechanisms of the electromagnetic radiation during rock fracture", *Acta Seismologica Sinica*, **10**(4), 86-94. https://doi.org/10.1007/s11589-997-0061-8.

Mori, Y., Obata, Y., Pavelka, J., Sikula, J. and Lokajicek, T. (2004), "AE Kaiser effect and electromagnetic emission in the deformation of rock sample", *J. Acoust. Emission*, **22**, 91-101.

Nardi, A. and Caputo, M. (2009), "Monitoring the mechanical stress of rocks through the electromagnetic emission produced by fracturing", *Int. J. Rock Mech. Min. Sci.*, **46**(5), 940-945.

Nitsan, U. (1977), "Electromagnetic emission accompanying fracture of quartz-bearing rocks", *Geophys. Res. Lett.*, **4**(8), 333-336. https://doi.org/10.1029/GL004i008p00333.

O'Keefe, S.G. and Thiel, D.V. (1995), "A mechanism for the production of electromagnetic radiation during fracture of brittle materials", *Phys. Earth Planet. Inter.*, **89**(1-2), 127-135. https://doi.org/10.1016/0031-9201(94)02994-M.

Ogawa, T., Oike, K. and Miura, T. (1985), "Electromagnetic radiation from rocks", *J. Geophys. Res. Atmosph.*, **90**(D4), 6245-6250. https://doi.org/10.1029/JD090iD04p06245.

Price, N.J, (1966), *Fault and Joint Development: in Brittle and Semi-brittle Rock*, Pergamon Press, Oxford, England, U.K.

Qian, S., Zhang, Y., Cao, H. and Zhi, A.L. (1986), "Electromagnetic Radiation Generated by the Rock Rupture During an Underground Explosion", *Acta Seismologica Sinica*.

Rabinovitch, A., Frid, V. and Bahat, D. (2007), "Surface oscillations—A possible source of fracture induced electromagnetic radiation", *Tectonophysics*, **431**(1-4), 15-21. https://doi.org/10.1016/j.tecto.2006.05.027.

Rabinovitch, A., Frid, V. and Bahat, D. (2017), "Directionality of electromagnetic radiation from fractures", *Int. J. Fracture*, **204**(2), 239-244. https://doi.org/10.1007/s10704-016-0178-7.

Rosen, B.W. (1964), "Tensile failure of fibrous composites", *AIAA J.*, **2**, 64-73. https://doi.org/10.2514/3.2699.

Sharma, S.K., Chauhan, V.S. and Kumar, A. (2016), "Detection of electromagnetic radiation in ferroelectric ceramics for non-contact sensing applications", *J. Alloys Compounds*, **662**, 534-540. https://doi.org/10.1016/j.jallcom.2015.12.026.

Song, D., Wang, E., He, X., Jia, H., Qiu, L., Chen, P., and Wang, S. (2018), "Use of electromagnetic radiation from fractures for mining-induced stress field assessment", *J. Geophys. Eng.*, **15**(4), 1093-1103. https://doi.org/10.1088/1742-2140/aaa26d.

Song, D., Wang, E., Li, Z., Qiu, L. and Xu, Z. (2017), "EMR: An effective method for monitoring and warning of rock burst hazard", *Geomech. Eng.*, **12**(1), 53-69. https://doi.org/10.12989/gae.2017.12.1.053.

Song, D., Wang, E., Song, X., Jin, P. and Qiu, L. (2016), "Changes in frequency of electromagnetic radiation from loaded coal rock", *Rock Mech. Rock Eng.*, **49**(1), 291-302. https://doi.org/10.1007/s00603-015-0738-6.

Wang, E., (1997), "The effect of EMR & AE during the fracture of coal containing gas and its applications", Ph.D. Dissertation, China University of Mining and Technology, Xuzhou, China.

Wang, E., He, X., Li, Z. and Zhao, E. (2009), *Electromagnetic Radiation Technology and Application of Coal or Rock*, Science Press, Beijing, China.

Yamada, T. and Oike, K. (1996), "Electromagnetic radiation phenomena before and after the 1995 Hyogo-ken Nanbu Earthquake", *Earth Planets Sp.*, **44**(4), 405-412. https://doi.org/10.4294/jpe1952.44.405.

Yavorovich, L.V., Bespalko, A.A., Fedotov, P.I. and Baksht, R.B. (2016), "Electromagnetic radiation generated by acoustic excitation of rock samples", *Acta Geophysica*, **64**(5), 1446-1461. https://doi.org/10.1515/acgeo-2016-0081.

Zhu, W., Chen, W. and Shen, J. (1998), "Simulation experiment and fracture mechanism study on propagation of Echelon pattern cracks", *Acta Mechanica Solida Sinica*, **19**, 355-360.

Zweben, C. and Rosen, B.W. (1970), "A statistical theory of material strength with application to composite materials", *J. Mech. Phys. Solids*, **18**(3), 189-206. https://doi.org/10.1016/0022-5096(70)90023-2.

CC